Paterson, Sureyya and Thompson, Sebastian A. and Wark, Alastair W. and de la Rica, Roberto (2017) Gold suprashells : enhanced photothermal nanoheaters with multiple LSPR for broadband SERS. Journal of Physical Chemistry C, 121 (13). pp. 7404-7411. ISSN 1932-7447 , http://dx.doi.org/10.1021/acs.jpcc.6b12792

This version is available at https://strathprints.strath.ac.uk/60147/

Gold Suprashells: Enhanced Photothermal Nanoheaters with Multiple LSPR for Broadband SERS

Sureyya Paterson,[1] Sebastian A. Thompson,[1,2] Alastair W. Wark,[1,] Roberto de la Rica[1,3,*]*

[1]WestCHEM, Department of Pure and Applied Chemistry, University of Strathclyde, Technology and Innovation Centre, 99 George Street, Glasgow, G1 1RD, Scotland, UK

[2] Department of Chemistry and Biochemistry, Hunter College - City University of New York, New York 10065, USA

[3] Department de Chemistry, University of the Balearic Islands, Camí de Valldemosa km 7.5, Palma de Mallorca, Illes Balears, Spain

ABSTRACT: In this manuscript we report on a new type of self-assembled plasmonic nanostructure called gold suprashells, which are assembled around superparamagnetic iron oxide nanoparticle (SPION) cores. Gold suprashells have multiple surface plasmon resonances over a broad vis-NIR wavelength range, which makes them useful in applications where broadband absorption is required. For example, suprashells are efficient substrates that enhance SERS signals across multiple excitation wavelengths. This unique multi-resonant character is afforded by the suprashell structure, which comprises anisotropic assemblies of nanoparticles of tunable length. Furthermore, gold suprashells generate more heat when excited with a laser compared to the nanoparticle building blocks, therefore making them promising materials for photothermal applications. The suprashells can potentially be assembled onto any negatively charged core, which opens up multiple possibilities for the development of multifunctional core/suprashell nanoparticle designs. Here, we assemble gold suprashells around dextran-coated SPIONs in order to obtain plasmonic and magnetic nanoparticles. Cells that have internalized the multifunctional nanoparticles can be accumulated with a magnet and killed with a laser through the generation of plasmonic heat. This approach shows promise for the development of therapies aimed at killing circulating tumor cells (CTCs) utilizing the proposed magnetic and plasmonic nanoparticles.

Gold nanoparticles are becoming indispensable tools in the nanomedicine toolbox due to their outstanding optical properties.[1] For example, the collective oscillations of electrons in the conduction band of these nanoparticles generate electric fields that enhance the Raman signals of molecules positioned close to their surface.[2,3] This observation is the basis of the surface-enhanced Raman scattering (SERS) technique,[4,5] which can be used for studying the intracellular delivery of nanomedicines,[6] tracking the biodistribution of drugs,[7] and determining the success of therapies *in vivo*.[8] Gold nanoparticles also generate heat when excited with light that is resonant with their localized surface plasmon resonance (LSPR).[9–13] Since nanoparticles accumulate easily in leaky tumors,[14] the plasmonic heat generated by gold nanostructures can be utilized to selectively kill cancer cells. However, great precision is required for *in vivo* SERS and photothermal therapy because these approaches require irradiating the tissue with a laser, which could easily kill healthy cells. Fortunately, the LSPR of gold nanoparticles can be tuned so that they absorb near infrared (NIR) light. In this spectral region biological components absorb less and lasers have a greater penetration depth.[15] Moreover, if nanoparticles generate highly intense electric fields, lasers of lower power and shorter irradiation times can be used to excite them. This makes NIR absorbers containing intense electric fields ideal for nanomedicine because they reduce side-effects originating from shining a laser on the target tissue.

Two strategies are commonly used to obtain plasmonic nanoparticles resonant in the NIR that generate highly intense electric fields. The first approach consists in assembling spherical nanoparticles into compact clusters.[16] This shifts their LSPR towards longer wavelengths and generates plasmonic "hot spots" in which the electric field is several orders of magnitude higher than in the nanoparticle building blocks (Fig. 1a (i) and (ii)).[17] The second approach requires growing anisotropic nanostructures, which generates NIR LSPR's and intensifies the electric

field at the nanoparticle vertices.[15,18] The main difference between these two nanostructures is that nanoparticle aggregates have broad and damped LSPR peaks whereas anisotropic nanoparticles have sharper resonances. In SERS, overlapping the extinction spectra of the nanoparticles and the target molecule results in more intense Raman signals.[19,20] This is easier to achieve when the LSPR is broad. However, sharp peaks allow the nanoparticles to absorb more light when excited with a laser resonant with their LSPR. In this context, a new nanoparticle design with efficient broadband absorption could become a versatile platform for SERS because it would support intense Raman signals of a wide range of molecules absorbing light at different wavelengths and when excited with different lasers. If the design included abundant hot spots, it could also improve photothermal applications, since the heat generated by plasmonic nanoparticles is directly proportional to the square of the electric field inside the metal.[21]

In this article we report a new self-assembled plasmonic nanostructure called gold suprashells that possesses multiple surface plasmon resonances over a broad Vis-NIR wavelength range. This multi-resonant character makes suprashells useful in applications where broadband absorption is required. Suprashells consist of a collection of anisotropic assemblies of nanoparticles supported on a negatively charged core (Fig. 1b). The anisotropic assemblies of gold nanoparticles have coupled surface plasmon resonances more similar to that of the longitudinal plasmon modes of gold nanorods than that associated with the random aggregation of spherical particles (Fig. 1a (iii)).[22–26] The absorbance wavelength of these coupled plasmon modes is intimately related to the length of the assemblies.[22–26] Suprashells are made of anisotropic assemblies containing different numbers of nanoparticle building blocks, which result in multiple surface resonances over a wide range of wavelengths. This makes gold suprashells a versatile platform for SERS spectroscopy regardless of the absorbance wavelength
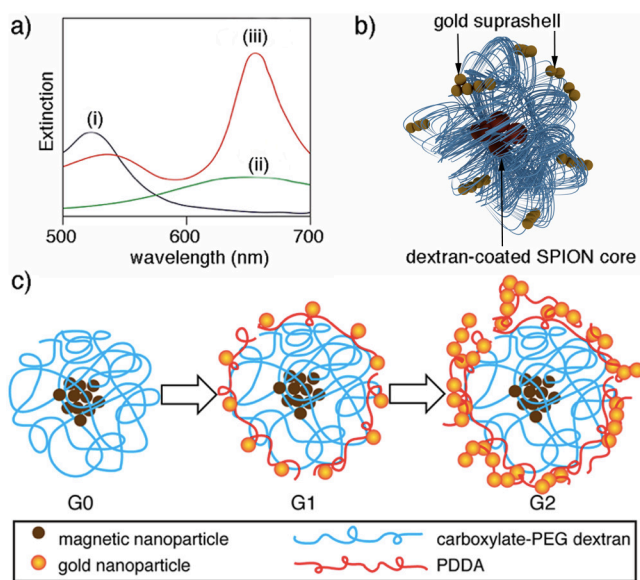
Figure 1. Schematic representation of (a) extinction spectrum of individual 20 nm gold nanoparticles (i); nanoparticle aggregates of uncontrolled morphology (ii), anisotropic assemblies of spherical nanoparticles (iii); (b) gold suprashells assembled on dextran-coated SPION; (c) Cross-sections showing the method used here to obtain gold suprashells. Anisotropic assemblies of nanoparticles in the suprashells are self-assembled by means of electrostatic interactions between positively charged PDDA molecules and negatively charged gold nanoparticles. Suprashells containing assemblies of different length are named with the code "GX", where X is the number of successive additions of PDDA and gold nanoparticles leading to more extended assemblies.

of the molecule under study.[27] Furthermore, gold suprashells generate more heat when excited with a laser compared to the individual nanoparticle building blocks, therefore making them promising materials for photothermal applications. The suprashells can potentially be assembled onto any negatively charged core, which opens up multiple possibilities for the development of

multifunctional core/suprashell nanoparticle designs. Here we assemble gold suprashells around dextran-coated superparamagnetic iron oxide nanoparticles (SPIONs) in order to obtain plasmonic and magnetic nanoparticles.[28–32] Cells that have internalized the multifunctional nanoparticles can be accumulated with a magnet and killed with a laser through the generation of plasmonic heat. This approach shows promise for the development of therapies aimed at killing circulating tumor cells (CTCs) utilizing the proposed magnetic and plasmonic nanoparticles.

RESULTS AND DISCUSSION

Figure 1c shows a scheme of the method used for assembling gold suprashells on SPION. The magnetic cores consist of iron oxide nanoparticles covered with dextran and are obtained from a commercial source. The dextran is modified with polyethylene glycol molecules (PEG) ending in carboxylate groups that confer negative charge to the nanoparticles (zeta potential (ζ) = -21.7 mV). Positively charged poly(diallyl-dimethylammonium) (PDDA) molecules are electrostatically wrapped around the cores, which changes their surface charge (ζ = 22.3 mV). After washing away the excess PDDA with water, citrate-capped gold nanoparticles are added (20 nm diameter, see Fig S1 in ESI). The positively charged PDDA molecules surrounding the SPION cores promote the adsorption of the negatively charged gold nanoparticles. Repeating the cycle of PDDA and gold nanoparticle additions promotes the formation of anisotropic assemblies, which increases the size of the suprashells (Figure S6). A possible mechanism for this could be based on the concept that following exposure to subsequent PDDA layers, the resulting PDDA coated nanoparticle forms a preferential adsorption site for the citrate-capped nanoparticles. Previous reports on the anisotropic assembly of gold nanoparticles with

polycations suggest that a nonuniform distribution of stabilizer ligands at different crystal faces has a directing role in the formation of such adsorption sites.[33] Suprashells created with repeat cycles of PDDA and gold nanoparticle building blocks are named "GX", where X is the number of successive additions of PDDA and gold nanoparticles.
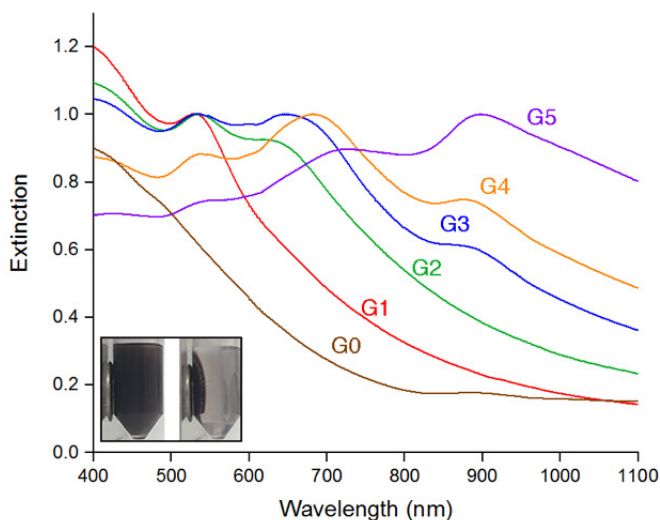

Figure 2. Vis-NIR spectra of G0 (brown), G1 (red), G2 (green), G3 (blue), G4 (orange) and G5 (purple); Inset: photographs of G3 in the presence of a magnet (left: t = 0 s, right: t = 90s).

Figure 2 shows vis-NIR spectra of the magnetic gold suprashells obtained with the procedure detailed in Figure 1c. All suprashells have a resonant peak at 530-540 nm, which corresponds to the LSPR of the gold nanoparticle building blocks (Fig. S1 in the Supporting Information). As the number of additional nanoparticle/polymer layers are increased from G1 to G5, new well-defined LSPR peaks emerge at increasingly red-shifted wavelengths extending into the NIR. The changing shapes of the extinction spectra with increasing layer number provides evidence of strong plasmonic coupling[17] with anisotropic assemblies of nanoparticles being favored on the

SPION surface rather than simple random aggregation. Recent theoretical and experimental [22,24–26] studies on quasi-linear or chain-like assemblies of Au nanospheres all demonstrate similar trends to that observed in Figure 2. As anisotropic assembly occurs, a relatively small ~10-15 nm red-shift and damping of the LSPR peak at ~530 nm is accompanied with the emergence of a higher intensity extinction peak at longer wavelengths in the >650 nm range. In a manner analogous to gold nanorods, the relative heights and widths of the LSPR peaks formed on anisotropic assembly depends on the relative length (number of particles) and width (degree of linearity, branch formation). In contrast, isotropic 3D assemblies of nanoparticles would not be expected to exhibit a continual red-shift of a distinct LSPR peak into the NIR with increasing assembly size.[34] Additionally, it is possible that the spectral features observed in Figure 2 are also associated with higher order multipolar resonances. The observation of quadrupoles in far-field extinction spectra has been reported in non-spherical particles (e.g. cubes, rods[35]) and considerably larger spherical particles featuring a low size dispersity.[36] However, the excitation of multipoles in the smaller (~20 nm) coupled spherical nanoparticles in the bulk-solution measurements here will much more likely contribute to the broad background of the LSPR profile observed rather than be associated with distinct peaks.

There are some differences between previous reported studies on anisotropic nanoparticle assembly[22,24–26] and the measurements reported here. First, it should be pointed out that the close proximity of the nanoparticles to the larger SPION will have a significant broadening and damping effect on the LSPR spectrum (compared to assemblies in suspension or on a glass support), which can be seen by comparing the colloidal and G1 spectra in Figure S1. Also, as the layer number increases, second and third LSPR peaks emerge, both of which red-shift and change in relative intensities as the nanoparticle assembly continues. In particular, the latter most

red-shifted peak forms at >900 nm for the G5 sample, with a continued relative decrease in the ~530 nm peak. This behavior is evidence of increasing anisotropy as the layer number increases. The observation of multiple resonance peaks above a broad background reflects that the nanoparticle assembly is unlikely to be highly uniform across the entire SPION substrate. This results in a unique multi-resonant behavior over a wide range of wavelengths.
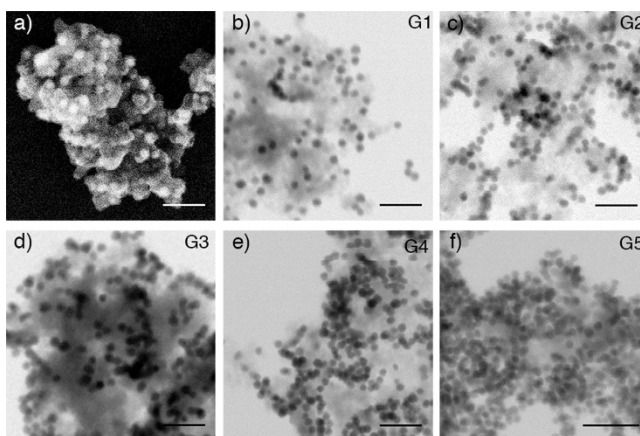

Figure 3. Electron microscopy images showing suprashells assembled on SPION; (a) In backscatter mode the contrast of the polymeric matrix is enhanced, which enables visualizing the overall shape of the dextran-coated SPION cores; (b), (c), (d), (e), and (f) correspond to G1, G2, G3, G4 and G5 in STEM mode, respectively. In these images the electron-dense gold nanoparticles can be easily identified by their characteristic size (20 nm). Scale bar: 100 nm.

Next, we studied the morphology of the suprashells with electron microscopy. The dextran around the SPION cores collapses under the high-vacuum conditions required for electron microscopy, which makes it challenging to visualize the exact morphology of the suprashells. In Figure 3a the dextran-coated cores of G3 were imaged in backscatter mode in order to maximize

the contrast of the polymeric matrix. In this image, the polymer-coated particles appear as undefined globular objects of low electron density. The particles have an average size of 500 nm as provided by the manufacturers and have irregular shapes. In Figs. 3b-3f, 20 nm gold nanoparticles can be clearly identified around the cores in scanning transmission electron microscopy (STEM) mode due to their characteristic size and electron density. In these images the number of gold nanoparticles per SPION core increases from G1 to G5, in agreement with the assembly method depicted in Fig. 1c. Although in some cases the nanoparticles seem to be randomly aggregated due to the collapse of the polymeric matrix, anisotropic assemblies can also be clearly detected, which are more extended as more nano-building blocks are assembled on the suprashell. These observations agree well with the plasmonic behavior of anisotropic assemblies of nanoparticles observed in Figure 2.

The observation of coupled plasmon modes in gold suprashells in Figure 2 demonstrates that the nanoparticle building blocks are assembled in close contact (the average inter-particle distance is 1.3 ± 0.3 nm, see Figure S2 in the Supporting Information). The presence of plasmonic hot spots resonant at multiple wavelengths could create a flexible platform capable of enhancing the Raman signal of molecules across a wide range of incident laser wavelengths, even when their absorbance wavelength does not match the LSPR of the nanoparticles. To demonstrate this concept G1, G3 and G5 gold suprashells were modified with 2-naphthalenethiol, a molecule that does not absorb vis-NIR light. Bulk SERS spectra were recorded upon excitation at 638 or 785 nm. All colloidal dispersions contained the same suprashell concentration ($1.4 \cdot 10^{10}$ particles$\cdot$mL^{-1}, calculated by nanoparticle tracking analysis). The resulting spectra were normalized to account for any instrumental variations in the signal intensity (see experimental section). In Figure 4, G1, G3 and G5 yield well-defined SERS
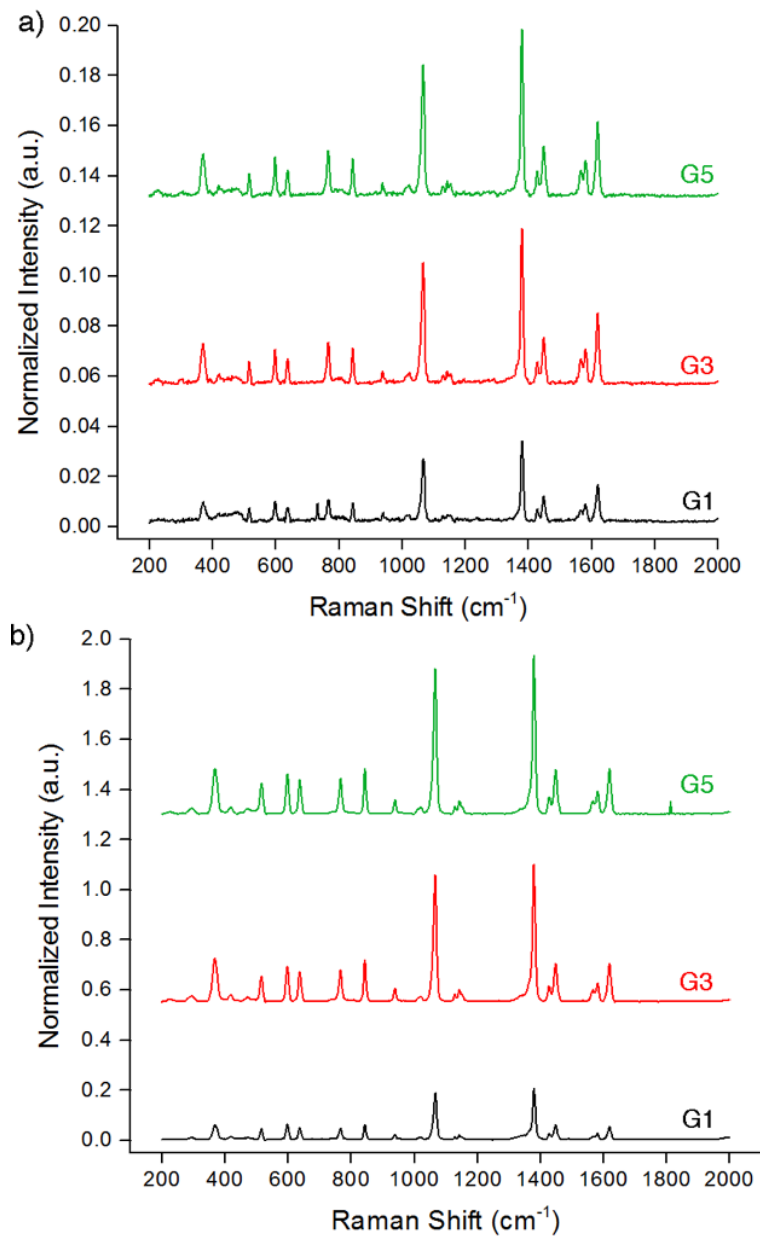
Figure 4. Bulk SERS spectra of G1 (black), G3 (red) and G5 (green) gold suprashells coated with 2-naphthalenethiol at excitation wavelengths of (a) 638 nm and (b) 785 nm. The concentration of suprashells in all samples was $1.4 \cdot 10^{10}$ particles·mL^{-1}. Spectra were normalized with respect to an ethanol spectrum taken in identical conditions.

spectra of 2-naphthalenethiol[37] irrespective of the excitation wavelength. Furthermore, the suprashells modified with the non-resonant Raman reporter can be detected at the single-suprashell level in SERS maps (Fig. S3 in the Supporting Information). This demonstrates that suprashells can yield detectable Raman signals even when the absorbance wavelength of the molecule under study does not match their LSPR. In all cases, the SERS intensities are ca. 10 times higher when the suprashells are excited at 785 nm compared to the same experiments performed at 638 nm. This observation is in line with previous studies reporting increased SERS enhancements as the excitation energy moves towards higher wavelengths.[38]

   The G3 and G5 samples always yield SERS signals that are more intense than G1 regardless of the excitation wavelength. During these measurements the particle densities were monitored (as determined by nanoparticle tracking analysis) to ensure that the differences in SERS intensities can be attributed to variation in the nanoparticle shell morphologies rather than the concentration of the suprashells. Thus, the lower G1 SERS signal can be attributed to a lower surface density of nanoparticles (and therefore hot spots) compared to G3 and G5. The SERS intensities obtained with G3 and G5 are very similar at the two wavelengths assayed even though the concentration of gold per suprashell is higher for G5 than for G3. This observation is in agreement with previous studies reporting that the enhancement factor in nanoparticle assemblies is not directly correlated to the number of constituent nanoparticle building blocks .[38] It also follows the general trend observed in theoretical studies such as that by Wang et al who report that the local electric field enhancement in linear particle assemblies is greatest in the central region of the assembly and the enhancement does not significantly increase further after the chain length goes beyond four particles in length.[39] Also, the SERS signal variation of a G5 sample was compared with that from a colloidal solution of individual NP building blocks

undergoing salt-induced aggregation. The latter was found to exhibit nearly twice the noise level

of the G5 sample, highlighting the advantage of kinetic stability also provided by the suprashell

approach. In summary, the results in Figure 4 demonstrate that the SERS response of gold

suprashells is dominated by the presence of hot spots.[40] The suprashells generate well-defined

SERS spectra of non-resonant molecules when excited at different wavelengths, even when

measured at the single-suprashell level. These features make gold suprashells excellent

candidates for multiplex analyses using several Raman reporters absorbing light at different

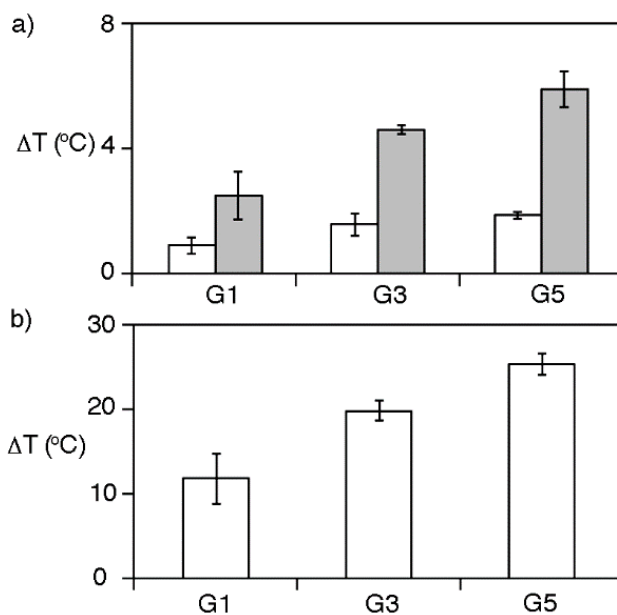wavelengths and attached to the same suprashell.[27]

Figure 5. Increase in temperature measured in suprashell dispersions after irradiating them with

a) a CW green laser (27 mW at the point of incidence) (white bars) or a CW NIR laser (27 mW

at the point of incidence) (gray bars); b) a CW NIR laser (235 mW at the point of incidence). The

concentration of gold in all experiments was 10 μM. Error bars are the standard deviation (n = 3).

Next we compared the generation of plasmonic heat by gold suprashells. G1, G3 and G5 suprashells were excited with two continuous wave (CW) lasers emitting light at either 514 or 785 nm. At the green excitation light, absorption is mainly related to the LSPR of the nanoparticle building blocks, whereas the coupled plasmon resonances absorb NIR light. The incident power was 27 mW for both lasers and focused into the samples. The concentration of gold, calculated by inductively coupled plasma mass spectrometry (ICP-MS), was 10 μM in all samples. The samples were irradiated for a short period of time to measure variations in the photothermal properties of the suprashells in the initial stages when the temperature of the solution changes linearly with time (see Fig. S4 in the Supporting Information). Figure 5a shows that, after irradiating the samples with the 514 nm laser for 1 min, the temperature increases more in the G3 and G5 suprashell dispersions than in G1. This means that G3 and G5 are more efficient nanoheaters compared to G1. The same trend was observed when exciting the nanoparticles with the 785 nm laser. It has been proposed that heat generation by plasmonic nanoparticles is directly proportional to the square of the electric field inside the metal.[21] Electric fields are intensified at hot spots.[17] Therefore we propose that the presence of a larger number of hot spots in G3 and G5 is the key factor for generating higher temperatures with these nanoheaters. Furthermore, the increase in temperature observed when exciting the suprashells with the NIR laser was ca. 3 times higher than when using the green laser. These experiments also suggest that the hot spots are the main contributors to heat generation. However it should be noted that other factors such as heat diffusion and heat distribution along the nanoparticle assemblies may also influence the temperature of the suprashell dispersion.[21,41,42] In Figure 5b the

785 nm laser power was increased to 235 mW. Under this condition higher increases in temperature were registered for all suprashells, which indicates that heat generation is also power-dependent (see also Figure S5 in the Supporting Information).

After studying the plasmonic properties of the gold suprashells we explored potential applications afforded by the magnetic core. The proposed gold suprashells assembled on SPION can be easily manipulated with a magnet (Fig. 1, inset). They are also internalized by cells and show low cytotoxicity *in vitro* (Figs. 6a-6b). Cells that have internalized the plasmonic and magnetic nanoparticles can be manipulated with a magnet (see Movie S1 in the Supporting Information). This led us to reason that gold suprashells assembled on SPION could potentially be used as nanomedicines for eliminating circulating tumor cells (CTCs). It is well established that the release of tumor cells into peripheral blood is a cause of cancer recurrence.[43,44] It is also a crucial factor in cancer metastasis.[45] In this context it would be desirable to design a therapeutic approach that could not only kill cancer cells at the primary tumor site but that also destroy cancer cells being shed into the blood stream. We propose that gold suprashells assembled on SPION could be used to this end when the CTCs bearing nanoparticles are accumulated with a magnet and killed with photothermal therapy. To test whether cells bearing suprashells can be accumulated with a magnet and killed with hyperthermia, suprashells were first dispersed in cell media followed by overnight incubation with prostate cancer cells. Dispersing the nanoparticles in cell media did not induce suprashell aggregation, which could affect cell internalization (Figure S7 in the Supporting Information). The next day cells were trypsinized and counted. Subsequently 76 ± 8% of the cells were accumulated with an external magnet and a cell pellet was formed. The pellet was then irradiated with a focused CW NIR laser (785 nm, 235 mW at the point of incidence), which would enable greater penetration depth in real healthcare

applications than the green laser. In Figure 6c, cells die after irradiating them with the laser for 5 min or longer, and
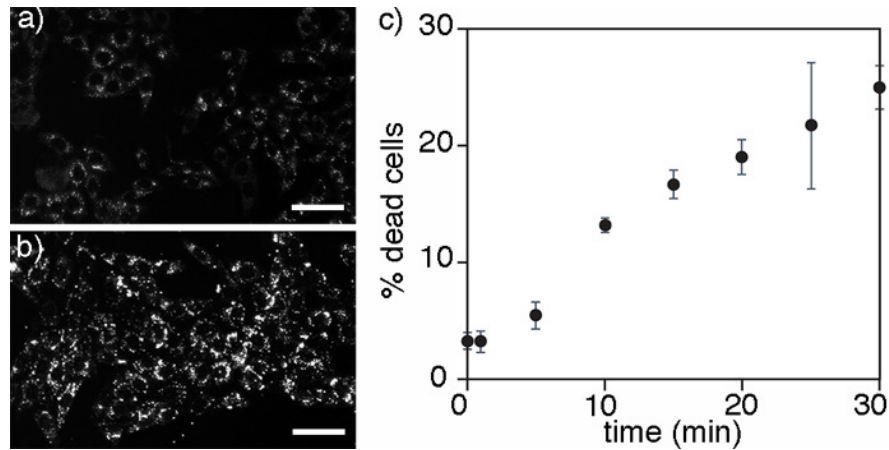

Figure 6. Dark-field microscopy images of prostate cancer cells; (a) without suprashells; (b) incubated with suprashells; nanoparticles are mainly found in the cell cytoplasm rather than in the nucleus; (c) Percentage of dead cells after irradiating a sample with a CW laser emitting light at 785 nm (75 mW at the point of incidence). The cells were incubated with magnetic and plasmonic suprashells and concentrated with a magnet prior to irradiation. Scale bars: 100 μm

T

he percentage of dead cells increase with irradiation time. This demonstrates the possibility of killing cancer cells with plasmonic heat after accumulating them with a magnet. Please note that the aim of these experiments was not killing all the cells in the pellet but rather showing that the cells can be killed with hyperthermia after magnetic accumulation. Only cells that come in contact with the laser beam are affected by the photothermal treatment. This means that the percentage of dead cells in Fig. 6 not only depends on the laser power and irradiation time but also on the diffusion of cells and relative volumes of the pellet and the laser irradiation, among

other factors. It should also be noted that the proposed suprashells do not selectively target cancer cells per se, and therefore that they should be modified with targeting moieties in order to be useful in cancer research. For example, suprashells could become selective nanomedicines for cancer research when modified with FDA-approved anti-EpCAM antibodies, which recognize CTCs.[46,47]

CONCLUSIONS

In conclusion, we have reported on a new type of self-assembled nanostructure called gold suprashells. Suprashells are multi-resonant at different wavelengths in the visible and NIR spectral range. This makes them versatile materials for applications that require exciting plasmonic nanoparticles over a wide range of wavelengths. Furthermore, they enable the Raman detection of molecules with single suprashell sensitivity. Another advantage of gold suprashells is that there is no need to modify the metal surface with protecting layers in order to prevent their aggregation in buffered solutions. This, along with their ability to boost SERS signals of molecules regardless of their absorbance wavelength, makes suprashells good candidates for identifying molecules by their Raman fingerprint as well.[48] The presence of hot spots also enhances the generation of heat by the gold suprashells. The generation of plasmonic heat can be used to kill cancer cells accumulated with a magnet after they have internalized the nanoparticles. This paves the way for the utilization of the proposed plasmonic and magnetic nanoparticles as therapeutic agents that enable ablating tumors and destroying circulating tumor cells with the same strategy. This is just one example of the many potential applications of the proposed magnetic and plasmonic nanoparticles. They could also be used in multimodal bioimaging strategies combining MRI and SERS,[49] in synergistic photothermal and

magnetothermal therapies,[50] or in cell sorting platforms combining magnetic manipulation and SERS detection.[51]

EXPERIMENTAL

Suprashell Assembly:

50 μL of dextran-coated SPION modified with PEG ending in carboxylate groups (10 mg·mL^{-1} (5.1·10^{10} particles mL^{-1}) micromod Partikeltechnologie GmbH) were added to 950 μL of 1% PDDA (diluted in Milli-Q water from a 35% stock solution, Sigma). After 20 min the samples were washed 4 times with water and 500 μL of gold nanoparticles (20 nm diameter, prepared via the Turkevich method[52] and concentrated by centrifugation to a concentration of 10 nM) were added to the SPIONs and left for 5 min followed by 4 additional washing steps. The addition of 500 μL of 1% PDDA and 500 μL of gold nanoparticles, each followed by 4 washing steps, was repeated to obtain G2 to G5 suprashells. The resulting solutions were diluted 5-fold and their vis-NIR spectra taken with a Cary 5000 spectrophotometer.

SERS

For the SERS experiments, 100 μL of 0.1 mM 2-napthalenethiol in ethanol (Sigma) was incubated overnight with 900 μL of the suprashell dispersion. All samples contained the same concentration of suprashells assembled on SPION, which was calculated via nanoparticle tracking analysis using a NanoSight LM10 (1.40 x 10^{10} particles mL^{-1}). The samples were then transferred to a glass vial where SERS spectra were obtained using two different Snowy Range Raman Spectrometers. The first instrument had an excitation wavelength of 638 nm and a spectral resolution of 8 cm^{-1} with an incident power set at 15 mW, and an integration time of 10 s

was used. The second instrument had an excitation wavelength of 785 nm and spectral resolution of 4 cm^{-1} with the laser power set to 15 mW and an integration time of 10 s. Background correction on all spectra was automatically calculated using the operating software (Peak).[53] Each spectrum was normalized with respect to an ethanol spectrum taken in identical conditions. This was done by dividing all spectra by the ethanol Raman peak intensity at 635 cm^{-1}.

Scanning electron microscopy

2 μL of sample was left to dry on a carbon-coated grid (Agar Scientific). SEM imaging was then performed with a FEI Quanta 250 FEG-ESEM at an acceleration voltage of 25 kW.

Cell culture and Nanoparticle Internalization

Prostatic small cell carcinoma (PC3) was kindly gifted from Professor Duncan Graham at the department of Pure and Applied Chemistry, University of Strathclyde. PC3 was grown in Dulbecco's modified Eagle's medium supplemented with 10% Fetal Bovine Serum (FBS). Cells were maintained at 37°C in a 5% CO_2 humidified environment. Cells were trypsinized and placed on glass slides or petri dishes for 2 days prior to imaging or photothermal experiments. For imaging experiments, cells were incubated with nanoparticles overnight or 36 h with nanoparticles (10 μl in 2 mL of medium). Incubations were performed in medium supplemented with 0.05% FBS. On the day of the experiment, the medium was removed and replaced with new medium. Cytotoxicity and cell death were studied with trypan blue or ethidium bromide following common protocols described elsewhere. They were determined to be lower than 5% after overnight incubation with a particle concentration of $7 \cdot 10^7$ particles·mL^{-1}. Transmission

dark-field microscopy images were obtained with a Nikon Eclipse LV100 with a 20x objective (Nikon S Plan Fluor ELWD, NA = 0.45).

Cell accumulation and photothermal experiments

To measure the increase in temperature triggered by plasmonic heat in suprashell dispersions, 20 μL of each sample was irradiated for 1 min with a CW laser (514 nm or 785 nm excitation wavelength, 27 mW at the point of incidence or 235 mW at the point of incidence (785 nm)). The laser was focused into the sample with a 30 cm focal length PCX lens (514 nm) or with a 50 cm focal length PCX lens (785 nm). The temperature in the drop was measured with a thermocouple (Digital Meter, model 6802 II), which is a validated method for studying light-to-heat conversion in solutions of gold nanoparticles.[54] Cells were killed with plasmonic heat with the following procedure. The day of the experiments, cells already incubated overnight with nanoparticles were trypsinized and centrifuged 3 times for 5 min at 96 g. The cells were re-suspended in fresh complete medium (4 mL) in a 10 mL tube and a magnet was externally placed in contact with the tube. The tube together with the magnet were placed on an orbital shaker for 5 min. Then, the medium was removed and recovered cells were re-suspended in 1 mL fresh medium and counted. For photothermal experiments, cancer cell pellets were formed by centrifugation and the medium was removed. A CW laser (785 nm, 235 mW at the point of incidence) was used to irradiate the cell pellet for different times (2, 5, 10, 15, 20, 25 and 30 min). Two controls were performed: cells without nanoparticles and 15 min irradiation time and cells with nanoparticles but no irradiation, which yielded $4.6 \pm 1\%$ and $4.8 \pm 1\%$ cell death, respectively. These controls suggest that the proposed irradiation conditions are suitable for in vivo models.

ASSOCIATED CONTENT

Supporting Information. Figures S1-S7, Movie S1

AUTHOR INFORMATION

Corresponding Author

*roberto.drica@uib.es, *alastair.wark@strath.ac.uk

Author Contributions

The manuscript was written through contributions of all authors. All authors have given approval

to the final version of the manuscript.

REFERENCES

(1)   Yohan, D.; Chithrani, B. D. Applications of Nanoparticles in Nanomedicine. *J. Biomed. Nanotechnol*. **2014**, *10* (9), 2371–2392.

(2)   Mirin, N. A.; Tamer, A. A.; Nordlander, P.; Halas, N. J. Perforated Semishells: Far-Field Directional Control and Optical Frequency Magnetic Response. *ACS Nano* **2010**, *4* (5), 2701–2712.

(3)   Wang, H.; Brandl, D. W.; Le, F.; Nordlander, P.; Halas, N. J. Nanorice: A Hybrid Plasmonic Nanostructure. *Nano Lett*. **2006**, *6* (4), 827–832.

(4)   Liu, D.; Li, C.; Zhou, F.; Zhang, T.; Zhang, H.; Li, X.; Duan, G.; Cai, W.; Li, Y. Rapid Synthesis of Monodisperse Au Nanospheres through a Laser Irradiation -Induced Shape Conversion, Self-Assembly and Their Electromagnetic Coupling SERS Enhancement. *Sci. Rep.* **2015**, *5*, 7686.

(5)   Zhang, H.; Liu, M.; Zhou, F.; Liu, D.; Liu, G.; Duan, G.; Cai, W.; Li, Y. Physical Deposition Improved SERS Stability of Morphology Controlled Periodic Micro/nanostructured Arrays Based on Colloidal Templates. *Small* **2015**, *11* (7), 844–853.

(6)   Yang, M.; Alvarez-Puebla, R.; Kim, H. S.; Aldeanueva-Potel, P.; Liz-Marzán, L. M.; Kotov, N. A. SERS-Active Gold Lace Nanoshells with Built-in Hotspots. *Nano Lett.* **2010**, *10* (10), 4013–4019.

(7)   Zavaleta, C. L.; Garai, E.; Liu, J. T. C.; Sensarn, S.; Mandella, M. J.; Van de Sompel, D.; Friedland, S.; Van Dam, J.; Contag, C. H.; Gambhir, S. S. A Raman-Based Endoscopic Strategy for Multiplexed Molecular Imaging. *Proc. Natl. Acad. Sci. U. S. A.* **2013**, *110* (25), E2288–E2297.

(8)   Jokerst, J. V.; Cole, A. J.; Van De Sompel, D.; Gambhir, S. S. Gold Nanorods for Ovarian Cancer Detection with Photoacoustic Imaging and Resection Guidance via Raman Imaging in Living Mice. *ACS Nano* **2012**, *6* (11), 10366–10377.

(9)   Donner, J. S.; Thompson, S. A.; Kreuzer, M. P.; Baffou, G.; Quidant, R. Mapping Intracellular Temperature Using Green Fluorescent Protein. *Nano Lett.* **2012**, *12*, 2107–2111.

(10)   Loo, C.; Lowery, A.; Halas, N.; West, J.; Drezek, R. Immunotargeted Nanoshells for

Integrated Cancer Imaging and Therapy. *Nano Lett.* **2005**, *5* (4), 709–711.

(11) Huang, X.; El-Sayed, I. H.; Qian, W.; El-Sayed, M. A. Cancer Cell Imaging and Photothermal Therapy in the near-Infrared Region by Using Gold Nanorods. *J. Am. Chem. Soc.* **2006**, *128* (6), 2115–2120.

(12) Donner, J. S.; Thompson, S. A.; Alonso-Ortega, C.; Morales, J.; Rico, L. G.; Santos, S. I. C. O.; Quidant, R. Imaging of Plasmonic Heating in a Living Organism. *ACS Nano* **2013**, *7* (10), 8666–8672.

(13) Cole, J. R.; Mirin, N. A.; Knight, M. W.; Goodrich, G. P.; Halas, N. J. Photothermal Efficiencies of Nanoshells and Nanorods for Clinical Therapeutic Applications. *J. Phys. Chem. C* **2009**, *113* (28), 12090–12094.

(14) Yu, M.; Zheng, J. Clearance Pathways and Tumor Targeting of Imaging Nanoparticles. *ACS Nano* **2015**, *9* (7), 6655–6674.

(15) Tsai, M. F.; Chang, S. H. G.; Cheng, F. Y.; Shanmugam, V.; Cheng, Y. S.; Su, C. H.; Yeh, C. S. Au Nanorod Design as Light-Absorber in the First and Second Biological near-Infrared Windows for in Vivo Photothermal Therapy. *ACS Nano* **2013**, *7* (6), 5330–5342.

(16) Ma, L. L.; Feldman, M. D.; Tam, J. M.; Paranjape, A. S.; Cheruku, K. K.; Larson, T. A.; Tam, J. O.; Ingram, D. R.; Paramita, V.; Villard, J. W.; et al. Small Multifunctional Nanoclusters (Nanoroses) for Targeted Cellular Imaging and Therapy. *ACS Nano* **2009**, *3* (9), 2686–2696.

(17) Halas, N. J.; Lal, S.; Chang, W.; Link, S.; Nordlander, P. Plasmons in Strongly Coupled

Metallic Nanostructures. *Chem. Rev.* **2011**, *111*, 3913–3961.

(18)   Kumar, P. S.; Pastoriza-Santos, I.; Rodriguez-Gonzalez, B.; Garcia de Abajo, F. J.; Liz-Marzan, L. M. High-Yield Synthesis and Optical Response of Gold Nanostars. *Nanotechnology* **2008**, *19* (1), 15606.

(19)   Liu, D.; Zhou, F.; Li, C.; Zhang, T.; Zhang, H.; Cai, W.; Li, Y. Black Gold: Plasmonic Colloidosomes with Broadband Absorption Self-Assembled from Monodispersed Gold Nanospheres by Using a Reverse Emulsion System. *Angew. Chemie - Int. Ed.* **2015**, *54* (33), 9596–9600.

(20)   Zhang, L.; Chang, H.; Hirata, A.; Wu, H.; Xue, Q. K.; Chen, M. Nanoporous Gold Based Optical Sensor for Sub-Ppt Detection of Mercury Ions. *ACS Nano* **2013**, *7* (5), 4595–4600.

(21)   Baffou, G.; Quidant, R. Thermo-Plasmonics: Using Metallic Nanostructures as Nano-Sources of Heat. *Laser Photonics Rev.* **2013**, *7* (2), 171–187.

(22)   Tira, C.; Tira, D.; Simon, T.; Astilean, S. Finite-Difference Time-Domain (FDTD) Design of Gold Nanoparticle Chains with Specific Surface Plasmon Resonance. *J. Mol. Struct.* **2014**, *1072* (1), 137–143.

(23)   Guo, L.; Ferhan, A. R.; Chen, H.; Li, C.; Chen, G.; Hong, S.; Kim, D. H. Distance-Mediated Plasmonic Dimers for Reusable Colorimetric Switches: A Measurable Peak Shift of More than 60 Nm. *Small* **2013**, *9* (2), 234–240.

(24)   Chang, W.-S.; Willingham, B. A.; Slaughter, L. S.; Khanal, B. P.; Vigderman, L.; Zubarev, E. R.; Link, S. Low Absorption Losses of Strongly Coupled Surface Plasmons in

Nanoparticle Assemblies. *Proc. Natl. Acad. Sci. U. S. A.* **2011**, *108* (50), 19879–19884.

(25) Zhang, H.; Wang, D. Controlling the Growth of Charged-Nanoparticle Chains through Interparticle Electrostatic Repulsion. *Angew. Chemie - Int. Ed.* **2008**, *47* (21), 3984–3987.

(26) Yin, Z.; Zhang, W.; Fu, Q.; Yue, H.; Wei, W.; Tang, P.; Li, W.; Li, W.; Lin, L.; Ma, G.; et al. Construction of Stable Chainlike Au Nanostructures via Silica Coating and Exploration for Potential Photothermal Therapy. *Small* **2014**, *10* (18), 3619–3624.

(27) McLintock, A.; Cunha-Matos, C. A.; Zagnoni, M.; Millington, O. R.; Wark, A. W. Universal Surface-Enhanced Raman Tags: Individual Nanorods for Measurements from the Visible to the Infrared (514-1064 Nm). *ACS Nano* **2014**, *8* (8), 8600–8609.

(28) Fan, Z.; Shelton, M.; Singh, A. K.; Senapati, D.; Khan, S. A.; Ray, P. C. Multifunctional Plasmonic Shell-Magnetic Core Nanoparticles for Targeted Diagnostics, Isolation, and Photothermal Destruction of Tumor Cells. *ACS Nano* **2012**, *6* (2), 1065–1073.

(29) Goon, I. Y.; Lai, L. M. H.; Lim, M.; Munroe, P.; Gooding, J. J.; Amal, R. Fabrication and Dispersion of Gold-Shell-Protected Magnetite Nanoparticles: Systematic Control Using Polyethyleneimine. *Chem. Mater.* **2009**, *21* (4), 673–681.

(30) Levin, C. S.; Hofmann, C.; Ali, T. a; Kelly, a T.; Morosan, E.; Nordlander, P.; Whitmire, K. H.; Halas, N. J. Magnetic– Plasmonic Core– Shell Nanoparticles. *ACS Nano* **2009**, *3* (6), 1379–1388.

(31) Li, C.; Chen, T.; Ocsoy, I.; Zhu, G.; Yasun, E.; You, M.; Wu, C.; Zheng, J.; Song, E.; Huang, C. Z.; et al. Gold-Coated Fe3O4 Nanoroses with Five Unique Functions for

Cancer Cell Targeting, Imaging, and Therapy. *Adv*. *Funct*. *Mater*. **2014**, *24* (12), 1772–1780.

(32) Yu, S.; Hachtel, J. A.; Chisholm, M. F.; Pantelides, S. T.; Laromaine, A.; Roig, A. Magnetic Gold Nanotriangles by Microwave-Assisted Polyol Synthesis. *Nanoscale* **2015**, *7* (33), 14039–14046.

(33) Wu, L.; Shi, C.; Tian, L.; Zhu, J. A One-Pot Method to Prepare Gold Nanoparticle Chains with Chitosan. *J*. *Phys*. *Chem*. *C* **2008**, *112* (2), 319–323.

(34) Urban, A. S.; Shen, X.; Wang, Y.; Large, N.; Wang, H.; Knight, M. W.; Nordlander, P.; Chen, H.; Halas, N. J. Three-Dimensional Plasmonic Nanoclusters. *Nano Lett*. **2013**, *13* (9), 4399–4403.

(35) Payne, E. K.; Shuford, K. L.; Park, S.; Schatz, G. C.; Mirkin, C. A. Multipole Plasmon Resonances in Gold Nanorods. *J*. *Phys*. *Chem*. *B* **2006**, *110* (5), 2150–2154.

(36) Bastús, N. G.; Piella, J.; Puntes, V. Quantifying the Sensitivity of Multipolar (Dipolar, Quadrupolar, and Octapolar) Surface Plasmon Resonances in Silver Nanoparticles: The Effect of Size, Composition, and Surface Coating. *Langmuir* **2016**, *32* (1), 290–300.

(37) Alvarez-Puebla, R. A.; Aroca, R. F. Synthesis of Silver Nanoparticles with Controllable Surface Charge and Their Application to Surface-Enhanced Raman Scattering. *Anal*. *Chem*. **2009**, *81* (6), 2280–2285.

(38) Kleinman, S. L.; Sharma, B.; Blaber, M. G.; Henry, A.; Valley, N.; Gri, R.; Natan, M. J.; Schatz, G. C.; Duyne, R. P. Van. Structure Enhancement Factor Relationships in Single

Gold Nanoantennas by Surface-Enhanced Raman Excitation Spectroscopy. *J. Am. Chem. Soc.* **2013**, *135*, 301–308.

(39) Wang, Z. B.; Luk'yanchuk, B. S.; Guo, W.; Edwardson, S. P.; Whitehead, D. J.; Li, L.; Liu, Z.; Watkins, K. G. The Influences of Particle Number on Hot Spots in Strongly Coupled Metal Nanoparticles Chain. *J. Chem. Phys.* **2008**, *128* (9).

(40) Popp, P. S.; Herrmann, J. F.; Fritz, E.-C.; Ravoo, B. J.; Höppener, C. Impact of the Nanoscale Gap Morphology on the Plasmon Coupling in Asymmetric Nanoparticle Dimer Antennas. *Small* **2016**, *12*, 1667–1675.

(41) Baffou, G.; Quidant, R.; García De Abajo, F. J. Nanoscale Control of Optical Heating in Complex Plasmonic Systems. *ACS Nano* **2010**, *4* (2), 709–716.

(42) Baldwin, C. L.; Bigelow, N. W.; Masiello, D. J. Thermal Signatures of Plasmonic Fano Interferences: Toward the Achievement of Nanolocalized Temperature Manipulation. *J. Phys. Chem. Lett.* **2014**, *5* (8), 1347–1354.

(43) Bayarri-Lara, C.; Ortega, F. G.; Cueto Ladrón de Guevara, A.; Puche, J. L.; Ruiz Zafra, J.; de Miguel-Pérez, D.; Ramos, A. S.-P.; Giraldo-Ospina, C. F.; Navajas Gómez, J. A.; Delgado-Rodriguez, M.; et al. Circulating Tumor Cells Identify Early Recurrence in Patients with Non-Small Cell Lung Cancer Undergoing Radical Resection. *PLoS One* **2016**, *11* (2), e0148659.

(44) Hall, C. S.; Karhade, M.; Laubacher, B. A.; Kuerer, H. M.; Krishnamurthy, S.; DeSnyder, S.; Anderson, A. E.; Valero, V.; Ueno, N. T.; Li, Y.; et al. Circulating Tumor Cells and Recurrence After Primary Systemic Therapy in Stage III Inflammatory Breast Cancer. *J.*

Natl. *Cancer Inst*. **2015**, *107* (11), 11–14.

(45)   Yoon, H. J.; Kozminsky, M.; Nagrath, S. Emerging Role of Nanomaterials in Circulating Tumor Cell Isolation and Analysis. *ACS Nano* **2014**, *8* (3), 1995–2017.

(46)   Chavva, S. R.; Pramanik, A.; Nellore, B. P. V; Sinha, S. S.; Yust, B.; Kanchanapally, R.; Fan, Z.; Crouch, R. A.; Singh, A. K.; Neyland, B.; et al. Theranostic Graphene Oxide for Prostate Cancer Detection and Treatment. *Part*. *Part*. *Syst*. *Charact*. **2014**, *31* (12), 1252–1259.

(47)   Wu, C.-H.; Cook, J.; Emelianov, S.; Sokolov, K. Multimodal Magneto-Plasmonic Nanoclusters for Biomedical Applications. *Adv*. *Funct*. *Mater*. **2014**, *24* (43), 6862–6871.

(48)   Huefner, A.; Kuan, W.-L.; Müller, K. H.; Skepper, J. N.; Barker, R. a.; Mahajan, S. Characterization and Visualization of Vesicles in the Endo-Lysosomal Pathway with Surface-Enhanced Raman Spectroscopy and Chemometrics. *ACS Nano* **2016**, *10*, 307−316.

(49)   Basiruddin, S. K.; Maity, A. R.; Saha, A.; Jana, N. R. Gold-Nanorod-Based Hybrid Cellular Probe with Multifunctional Properties. *J*. *Phys*. *Chem*. *C* **2011**, *115* (40), 19612–19620.

(50)   Wo, F.; Xu, R.; Shao, Y.; Zhang, Z.; Chu, M.; Shi, D.; Liu, S. A Multimodal System with Synergistic Effects of Magneto-Mechanical, Photothermal, Photodynamic and Chemo Therapies of Cancer in Graphene-Quantum Dot-Coated Hollow Magnetic Nanospheres. *Theranostics* **2016**, *6* (4), 485–500.

(51)   Pallaoro, A.; Hoonejani, M. R.; Braun, G. B.; Meinhart, C. D.; Moskovits, M. Rapid Identification by Surface-Enhanced Raman Spectroscopy of Cancer Cells at Low Concentrations Flowing in a Microfluidic Channel. *ACS Nano* **2015**, *4* (4), 4328–4336.

(52)   Kimling, J.; Maier, M.; Okenve, V.; Kotaidis, V.; Ballot, H.; Plech, a; Okenve, B. Turkevitch Method for Gold Nanoparticle Synthesis Revisited. *J. Phys. Chem. B* **2006**, *110* (95 mL), 15700–15707.

(53)   Mosier-Boss, P. A.; Putnam, M. D. The Evaluation of Two Commercially Available, Portable Raman Systems. *Anal. Chem. Insights* **2013**, *8* (1), 83–97.

(54)   Richardson, H. H.; Carlson, M. T.; Tandler, P. J.; Hernandez, P.; Govorov, A. O. Experimental and Theoretical Studies of Light-to-Heat Conversion and Collective Heating Effects in Metal Nanoparticle Solution. *Nano Lett.* **2009**, *9* (3), 1139–1146.